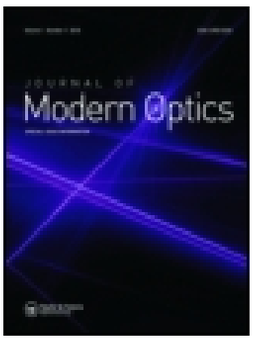

Journal of Modern Optics

ISSN: 0950-0340 (Print) 1362-3044 (Online) Journal homepage: http://www.tandfonline.com/loi/tmop20

Ultrashort polarization-tailored bichromatic fields

Stefanie Kerbstadt, Lars Englert, Tim Bayer & Matthias Wollenhaupt

To cite this article: Stefanie Kerbstadt, Lars Englert, Tim Bayer & Matthias Wollenhaupt (2016): Ultrashort polarization-tailored bichromatic fields, Journal of Modern Optics, DOI: 10.1080/09500340.2016.1271151

To link to this article: http://dx.doi.org/10.1080/09500340.2016.1271151

JOURNAL OF MODERN OPTICS, 2016
http://dx.doi.org/10.1080/09500340.2016.1271151

Taylor & Francis
Taylor & Francis Group

Ultrashort polarization-tailored bichromatic fields

Stefanie Kerbstadt, Lars Englert, Tim Bayer and Matthias Wollenhaupt

Institute of physics, Carl-von-Ossietzky-University of Oldenburg, Oldenburg, Germany

ABSTRACT

We present a novel concept for the generation of ultrashort polarization-shaped bichromatic laser fields. The scheme utilizes a 4*f* polarization pulse shaper based on a liquid crystal spatial light modulator for independent amplitude and phase modulation of femtosecond laser pulses. By choice of either a conventional (*p*) or a composite (*p*-*s*) polarizer in the Fourier plane, the shaper setup enables the generation of parallel linearly and orthogonal linearly polarized bichromatic fields. Additional use of a $\lambda/4$ wave plate behind the setup yields co-rotating and counter-rotating circularly polarized bichromatic fields. The scheme allows to independently control the spectral amplitude, phase and polarization profile of the output fields, offering an enormous versatility of bichromatic waveforms.

ARTICLE HISTORY
Received 26 September 2016
Accepted 21 November 2016

KEYWORDS
Tailored femtosecond laser pulses; bichromatic fields; ultrafast polarization shaping; shaper-based pulse characterization; white light supercontinuum; ultrafast electron dynamics

1. Introduction

The ability to control the electric field of ultrashort laser pulses on a sub-cycle level has opened up exciting new perspectives for the generation of tailored waveforms to steer ultrafast quantum dynamics on their intrinsic timescales. In particular, direct manipulation of ultrafast electron dynamics on the sub-femtosecond (fs) to attosecond (as) timescale has become feasible with the advent of waveform-controlled fs-pulses (*1*–*5*). Recently, bichromatic laser fields with adjustable state of polarization of each colour have emerged as a powerful tool to control coherent electron dynamics in various applications, comprising strong-field ionization of atoms (*6*–*10*), high harmonic generation (*11*–*17*), charge localization in ultrafast photochemical reactions (*18*, *19*) and phase control of electric currents in semiconductors (*20*, *21*) and metals (*22*). The physical mechanism behind bichromatic control is the interference of *n*- vs. *m*-photon pathways, with *n* and *m* being integer numbers (*23*). When both *n* and *m* are odd (or even) the excitation yield can be controlled by adjustment of the relative phase between the two interfering quantum pathways. Choosing *n* to be odd and *m* to be even (or vice versa) allows to manipulate the angular distribution of the excited electrons via the interference of quantum states with different parity. Using polarization-shaped bichromatic fields in multiphoton schemes, additionally enables selective excitation through exploitation of dipole selection rules and resonances.

So far, bichromatic laser fields have typically been generated by superimposing the fundamental laser beam, e.g. from a Ti:Sa laser source, and its second harmonic using an interferometer, optionally equipped with a $\lambda/4$ wave plate (QWP) in each arm to separately control the polarization of both colours. In this paper we present an alternative route to the generation of ultrashort polarization-shaped bichromatic fields based on a common-path setup (*24*–*28*) replacing the interferometer and, therefore, providing inherent phase stability of both colours. The scheme utilizes a 4*f* polarization shaper (*29*) for independent phase and amplitude shaping to sculpture the desired bichromatic amplitude profile from a broadband input spectrum. Additional spectral phase modulation allows to tailor the temporal shape of both colours individually. The polarization of each colour is controlled in the Fourier plane of the 4*f* setup by using a composite polarizer with specific transmission directions for different spectral bands. This enables, for example, the generation of orthogonal linearly and – by additional use of a QWP – counter-rotating circularly polarized (CNR-CP) bichromatic fields, both of which is challenging in traditional fs pulse shaping (*29*–*31*). Recently, other common-path setups have been proposed for full control over the electric field of fs laser pulses (*26*, *27*, *32*). While strategies relying on more than two Liquid Crystal Displays (LCDs) (*26*, *32*, *33*) are prohibitively expensive, the approach introduced by Brixner et al. (*27*, *34*, *35*) has several advantages. For

CONTACT Matthias Wollenhaupt matthias.wollenhaupt@uni-oldenburg.de

ultra-broadband applications, such as the generation of few-cycle bichromatic fields extracted from a white light supercontinuum (WLS) (see discussion in Section 4) the reduced spectral resolution (factor 2) might however be unfavourable. The scheme presented here is specifically tailored to the generation of polarization-shaped bichromatic waveforms. The concept to independently shape two separate spectral bands rather than one broadband input field is expressed not only by the use of a composite polarizer, i.e. the individual treatment of two colours in the Fourier plane, but also by introducing a bichromatic pulse parameterization which describes the spectral shape of both colours independently in terms of two individual phase and amplitude functions. The choice of a canonical spectral description greatly facilitates the conceptual understanding of the resulting pulse shapes in time-domain.

The paper is organized as follows. We start in Section 2 by developing the theoretical background for the shaper-based generation and characterization of polarization-tailored bichromatic fields. Based on the bichromatic pulse parameterization we derive explicit analytical expressions for the phase modulation functions applied to the LCDs in order to implement the scheme experimentally. In Section 3 we present the experimental setup and results. After a proof of concept we systematically explore different modes of the shaper-based generation and characterization of polarization-shaped bichromatic fields. In Section 4 we apply the scheme to a WLS and demonstrate the generation of ultrashort bichromatic fields with (low order) commensurable frequencies. The paper concludes with a brief summary and outlook.

2. Theoretical description

In this section, we introduce our concept for the generation of polarization-shaped ultrashort bichromatic fields with tailored spectral amplitude and phase profiles. The optical setup is based on a 4*f* polarization pulse shaper equipped with a dual-layer Liquid Crystal Spatial Light Modulator (LC-SLM) for independent phase modulation of two orthogonal input field components (±45°, shaper frame, see Figure 1). When a standard polarizer is placed behind the LC-SLM the setup realizes independent spectral amplitude and phase modulation of a linearly polarized field component. Using the polarization shaper in amplitude modulation mode allows to carve two-colour spectra from the input spectrum with any desired shape, ratio of central frequencies, widths and peak amplitudes supported by the available bandwidth. In addition, both spectral bands can independently be phase-modulated, resulting in amplitude- and phase-tailored parallel linearly polarized (P-LP) bichromatic output fields. With these fields available, the generation of co-rotating circularly polarized (COR-CP) bichromatic fields is readily achieved using an additional QWP. The generation of either orthogonal linearly polarized (O-LP) or CNR-CP bichromatic fields is more demanding. To this end we conceived a novel scheme based on a composite polarizer consisting of two adjacent active areas with orthogonal transmission directions (*s* and *p*, laboratory frame) as displayed in Figure 1. With this modification the setup allows to modulate the amplitude and phase of two separated spectral bands with orthogonal polarization directions, yielding shaped bichromatic fields of orthogonal linear polarization. In this case, additional application of the QWP results in CNR-CP bichromatic fields (cf. Figure 1). Thus, utilizing a 4*f* polarization shaper in combination with a composite polarizer and a QWP all three degrees of freedom, i.e. spectral phase, amplitude and polarization, of the bichromatic field are accessible for independent modulation.

In the following Section 2.1, we develop the mathematical description for the shaper-based generation of bichromatic fields employing the Jones matrix formalism. In Section 2.2, we introduce a technique to characterize the bichromatic output fields, utilizing the polarization shaper as a tool to mimic the interferometer conventionally employed in ultrafast pulse diagnostics.

2.1. Shaper-based generation of polarization-tailored bichromatic fields

In this section, we derive explicit analytical expressions for the spectral phase modulation functions $\varphi_A(\omega)$ and $\varphi_B(\omega)$ applied to the LCDs A and B of the LC-SLM in order to implement bichromatic amplitude and phase modulation. To this end we first introduce the four basic polarization states of bichromatic fields with respect to the relative polarization of the two colours in Section 2.1.1. After the definition of a canonical pulse parameterization to suitably describe the modulated bichromatic output fields we present the optical implementation in Section 2.1.2.

2.1.1. Basic modes of bichromatic fields

Bichromatic fields can assume four basic states of polarization with respect to the relative polarization of the two colours. These states are (i) P-LP, (ii) O-LP, (iii) COR-CP and (iv) CNR-CP, as summarized in the inset to Figure 1. In view of the shaper-based generation of bichromatic fields it is sufficient to concentrate on states (i) and (ii), since states (iii) and (iv) are obtained from these by additional use of a QWP. For the mathematical description of these fields we consider an input laser pulse in the laboratory frame polarized along the *y*-axis

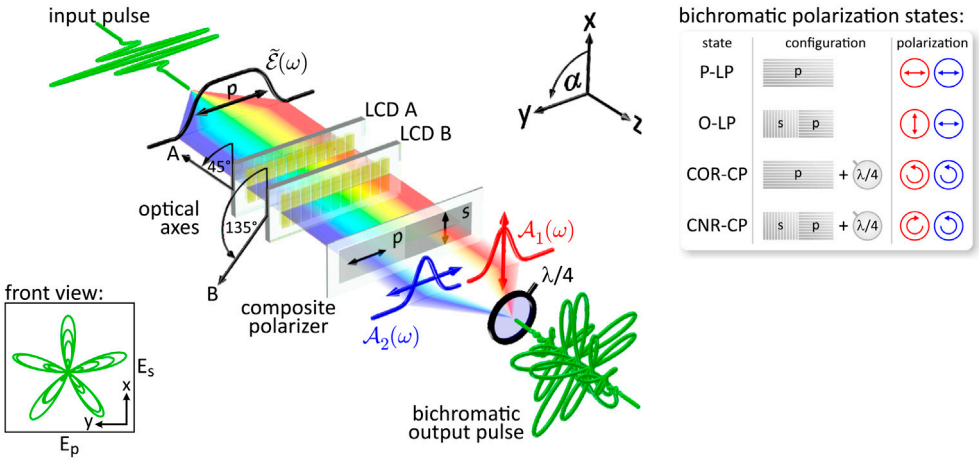

Figure 1. Schematic of the shaper-based scheme for generation of ultrashort polarization-tailored bichromatic laser fields. The *p*-polarized input pulse is spectrally dispersed and imaged into the Fourier plane of the 4*f* zero dispersion setup by a grating and focusing mirror (not shown). In the Fourier plane two sequential LC-masks, LCD A and B, with optical axes tilted by 45° with respect to the laboratory frame (*x*-*y*-plane), realize independent phase modulation of two orthogonal field components (shaper frame). Amplitude modulation is implemented by a polarizer placed behind LCD B. Using a composite polarizer, as shown in figure, the red part of the spectrum is projected onto *s*-, while the blue part is projected orthogonally onto *p*-direction. In this configuration the shaper delivers O-LP bichromatic fields with independently controllable amplitude and spectral phase of each colour. Conversion to CNR-CP fields is achieved by a QWP with fast axis aligned at $\alpha = \pm 45°$ behind the shaper. The right inset summarizes the different modes of the scheme. The figure exemplifies the concept on a bandwidth-limited CNR-CP field with a central frequency ratio of 2 : 3, which results in propeller-type pulses with five-fold symmetry as displayed in the left inset.

(*p*-direction) and travelling in *z*-direction (cf. Figure 1). The electric field of the input pulse is written in terms of its positive frequency analytic signal as

$$\boldsymbol{E}^{+}_{in}(t,z) = \mathcal{E}(t)e^{i(\omega_0 t - kz)}\begin{pmatrix}0\\1\end{pmatrix}, \tag{1}$$

with the temporal envelope $\mathcal{E}(t)$, the central frequency ω_0 and the wave number k. The following discussion focuses on the field envelopes in time and frequency domain. Therefore, both the spatial dependence e^{-ikz} and the carrier oscillation $e^{i\omega_0 t}$ are dropped in the notation. Let $\tilde{\boldsymbol{E}}^{+}_{in}(\omega)$ be the positive frequency spectrum of the input pulse and $\tilde{\mathcal{E}}(\omega)$ the Fourier transform of the envelope $\mathcal{E}(t)$. According to the Fourier shift theorem, the spectrum of the temporal envelope $\boldsymbol{\mathcal{E}}^{+}_{in}(t) = [0, \mathcal{E}(t)]^T$ is shifted by ω_0 and centered around $\omega = 0$. In vectorial representation the shifted spectrum is given by

$$\tilde{\boldsymbol{\mathcal{E}}}^{+}_{in}(\omega) = \tilde{\boldsymbol{E}}^{+}_{in}(\omega + \omega_0) = \tilde{\mathcal{E}}(\omega)\begin{pmatrix}0\\1\end{pmatrix}. \tag{2}$$

In the following (see Section 2.1.2) we describe how this input pulse is transformed into a target output pulse $\tilde{\boldsymbol{\mathcal{E}}}^{+}_{\text{out}}(\omega)$ consisting of two non-overlapping spectral bands (colours) with respective amplitudes $\mathcal{A}_1(\omega)$ centered around $\omega_1 < 0$ and $\mathcal{A}_2(\omega)$ centered around $\omega_2 > 0$. In addition, we allow for the individual spectral phase modulation of each colour via the corresponding phase modulation functions $\varphi_1(\omega)$ and $\varphi_2(\omega)$. In the case of P-LP bichromatic fields (case (i)) both colours are linearly polarized, e.g. in *p*-direction. Thus the target output field has the form $\tilde{\boldsymbol{\mathcal{E}}}^{+}_{\text{out,para}}(\omega) = [0, \tilde{\mathcal{E}}_{\text{out},p}(\omega)]^T$, with

$$\tilde{\mathcal{E}}_{\text{out},p}(\omega) = \begin{cases}\mathcal{A}_1(\omega)e^{-i\varphi_1(\omega)}, & \omega < 0\\ \mathcal{A}_2(\omega)e^{-i\varphi_2(\omega)}, & \omega \geq 0\end{cases}. \tag{3}$$

In the case of O-LP fields (case (ii)) both colours are also linearly polarized but in different directions, e.g. in *s*- and *p*-direction. This scenario is depicted in Figure 1. Here the output field is of the form $\tilde{\boldsymbol{\mathcal{E}}}^{+}_{\text{out,ortho}}(\omega) = [\tilde{\mathcal{E}}_{\text{out},s}(\omega), \tilde{\mathcal{E}}_{\text{out},p}(\omega)]^T$, with

$$\tilde{\mathcal{E}}_{\text{out},s}(\omega) = \begin{cases}\mathcal{A}_1(\omega)e^{-i\varphi_1(\omega)}, & \omega < 0\\ 0, & \omega \geq 0\end{cases} \quad \text{and}$$
$$\tilde{\mathcal{E}}_{\text{out},p}(\omega) = \begin{cases}0, & \omega < 0\\ \mathcal{A}_2(\omega)e^{-i\varphi_2(\omega)}, & \omega \geq 0\end{cases}. \tag{4}$$

Next we show how bichromatic fields as described by Equations (3) and (4) are implemented experimentally.

2.1.2. Optical implementation

The polarization shaper used for the implementation of the bichromatic fields in Equations (3) and (4) is based on a dual-layer LC-SLM with crossed optical axes (36). The

optical axes of LCD A and B constitute the shaper frame which is coplanar to the laboratory frame (x-y-plane) and tilted by $\alpha = 45°$ about the z-axis with respect to the x-axis (see Figure 1). Each display acts as a variable wave plate introducing the spectral phase retardations $\varphi_A(\omega)$ and $\varphi_B(\omega)$, respectively. Employing the Jones matrix formalism, the dual-layer LC-SLM is described by the matrix

$$\tilde{\mathcal{M}}(\omega) = \mathcal{R}(-\pi/4)\begin{pmatrix} e^{-i\varphi_A(\omega)} & 0 \\ 0 & e^{-i\varphi_B(\omega)} \end{pmatrix}\mathcal{R}(\pi/4),$$
$$\text{with} \quad \mathcal{R}(\alpha) = \begin{pmatrix} \cos(\alpha) & \sin(\alpha) \\ -\sin(\alpha) & \cos(\alpha) \end{pmatrix}. \tag{5}$$

Note, that in our notation the phase functions $\varphi_{A/B}(\omega)$ refer to the shifted spectrum and are therefore centered around $\omega = 0$, not around $\omega = \omega_0$. Then the modulated field reads

$$\tilde{\boldsymbol{\mathcal{E}}}^{+}_{mod}(\omega) = \tilde{\mathcal{M}}(\omega)\,\tilde{\boldsymbol{\mathcal{E}}}^{+}_{in}(\omega). \tag{6}$$

Equations (5) and (6) describe conventional phase and polarization modulation as discussed extensively in the literature (*26*, *29*, *36*–*39*). In order to implement amplitude modulation, e.g. for the design of specific bichromatic amplitude profiles, a polarizer is inserted behind the LC-SLM (*40*–*42*). For example, using a p-polarizer

$$\mathcal{P}_p = \begin{pmatrix} 0 & 0 \\ 0 & 1 \end{pmatrix} \tag{7}$$

allows to generate P-LP bichromatic fields (case (i)) polarized in p-direction. Multiplication of Equation (6) by Equation (7) and using the phase modulation functions

$$\varphi_A(\omega) = \varphi(\omega) + \operatorname{acos}\left(\frac{\mathcal{A}(\omega)}{\tilde{\mathcal{E}}(\omega)}\right) \qquad \text{and}$$
$$\varphi_B(\omega) = \varphi(\omega) - \operatorname{acos}\left(\frac{\mathcal{A}(\omega)}{\tilde{\mathcal{E}}(\omega)}\right), \tag{8}$$

with

$$\varphi(\omega) = \begin{cases} \varphi_1(\omega), & \omega < 0 \\ \varphi_2(\omega), & \omega \geq 0 \end{cases} \qquad \text{and}$$
$$\mathcal{A}(\omega) = \begin{cases} \mathcal{A}_1(\omega), & \omega < 0 \\ \mathcal{A}_2(\omega), & \omega \geq 0 \end{cases}, \tag{9}$$

in Equation (5) deliver the linearly polarized bichromatic output field $\tilde{\boldsymbol{\mathcal{E}}}^{+}_{\text{out,para}}(\omega)$ as described by Equation (3). Additional application of a QWP, described by the Jones matrix

$$\Lambda_4(\alpha) = \mathcal{R}(-\alpha)\begin{pmatrix} 1 & 0 \\ 0 & e^{-i\pi/2} \end{pmatrix}\mathcal{R}(\alpha), \tag{10}$$

where α denotes the angle of the fast axis relative to the x-axis, yields COR-CP bichromatic fields (case (iii)) according to $\tilde{\boldsymbol{\mathcal{E}}}^{+}_{\text{out,co}}(\omega) = \Lambda_4(\pm\pi/4)\tilde{\boldsymbol{\mathcal{E}}}^{+}_{\text{out,para}}(\omega)$.

The generation of O-LP and CNR-CP bichromatic fields (cases (ii) and (iv)) is not readily implemented in traditional Fourier pulse shaping because it requires independent modulation of amplitude and polarization. To this end we introduce a novel concept based on a composite polarizer, as illustrated in Figure 1. The composite polarizer consists of two adjacent active areas with transmission directions aligned orthogonally in s- and p-direction, respectively. Inserted directly behind the LC-SLM each area covers one half of the input spectrum dividing the spectrum into two bands with orthogonal polarization directions. Making use of the Heaviside step function $\theta(\omega)$, the corresponding Jones matrix reads

$$\mathcal{P}_c(\omega) = \theta(-\omega)\mathcal{P}_s + \theta(\omega)\mathcal{P}_p$$
$$= \begin{pmatrix} \theta(-\omega) & 0 \\ 0 & \theta(\omega) \end{pmatrix}, \quad \text{with}$$
$$\mathcal{P}_s = \begin{pmatrix} 1 & 0 \\ 0 & 0 \end{pmatrix}. \tag{11}$$

Multiplication of Equation (6) by Equation (11) and using the phase modulation functions

$$\varphi_A(\omega) = \begin{cases} \varphi_1(\omega) - \operatorname{acos}\left(\frac{\mathcal{A}_1(\omega)}{\tilde{\mathcal{E}}(\omega)}\right), & \omega < 0 \\ \varphi_2(\omega) + \operatorname{acos}\left(\frac{\mathcal{A}_2(\omega)}{\tilde{\mathcal{E}}(\omega)}\right), & \omega \geq 0 \end{cases} \tag{12}$$

and

$$\varphi_B(\omega) = \begin{cases} \varphi_1(\omega) - \operatorname{acos}\left(-\frac{\mathcal{A}_1(\omega)}{\tilde{\mathcal{E}}(\omega)}\right), & \omega < 0 \\ \varphi_2(\omega) - \operatorname{acos}\left(\frac{\mathcal{A}_2(\omega)}{\tilde{\mathcal{E}}(\omega)}\right), & \omega \geq 0 \end{cases} \tag{13}$$

result in an O-LP bichromatic output field $\tilde{\boldsymbol{\mathcal{E}}}^{+}_{\text{out,ortho}}(\omega)$ as described by Equation (4). The apparent asymmetry of Equations (12) and (13) with respect to the sign of the acos-function arises from our choice of the shaper frame, in which the s-polarized red ($\omega < 0$) field component is projected onto the negative axis of LCD B. Finally, CNR-CP fields are generated by using the QWP from Equation (10) aligned at $\alpha = \pm\pi/4$ at the shaper output to obtain $\tilde{\boldsymbol{\mathcal{E}}}^{+}_{\text{out,counter}}(\omega) = \Lambda_4(\pm\pi/4)\tilde{\boldsymbol{\mathcal{E}}}^{+}_{\text{out,ortho}}(\omega)$.

2.2. Characterization of polarization-shaped bichromatic fields

In order to characterize the polarization-shaped bichromatic output fields we first measure the temporal profiles of two orthogonal polarization components employing a shaper-based spectrally resolved second order Cross-Correlation (CC) technique (*28*) (see Section 2.2.1).

Because the pulse to be analyzed consists of two spectrally separated bands, the CC exhibits an ambiguity with respect to relative phases between the two polarization components (*43*) and is thus not sensitive to the helicity of the pulse. Therefore the CC measurement is supplemented by an additional Spectral Interference (SI) measurement using a Mach–Zehnder interferometer behind the shaper output which reveals the circularity of each colour of the bichromatic field (see Section 2.2.2).

2.2.1. Shaper-based CC

For the implementation of the correlation measurement we utilize the polarization pulse shaper to mimic an interferometer (*24*, *25*, *28*, *42*). The time-delayed reference pulse is split off the input pulse via spectral phase and amplitude modulation. Due to the common-path geometry this type of scheme provides inherent phase stability between sample and reference pulse. Moreover, the time-delay can be adjusted with extreme precision down to the zeptosecond-regime (*42*). In the following, both the sample and the reference pulse are described by the spectrum of their respective temporal envelopes. For the reference pulse we choose a bandwidth-limited replica of the sample pulse. The time delay is realized via the modulation phase

$$\varphi_{ref}(\omega) = \gamma\pi + \begin{cases} \tau\cdot(\omega-\omega_{ref,1}), & \omega<0 \\ \tau\cdot(\omega-\omega_{ref,2}), & \omega\geq 0 \end{cases}. \tag{14}$$

Again, this expression is to be interpreted as the phase of the shifted reference pulse spectrum. The linear term in Equation (14) serves to shift the reference pulse in time by a variable delay τ. Applying the linear phase with respect to different reference frequencies $\omega_{ref,n}$ $(n=1,2)$ corresponds to different correlation modes (*28*). In a bichromatic scenario three particular modes are distinguished. The first mode is defined by $\omega_{ref,1}=\omega_{ref,2}=-\omega_0$ and $\gamma=0$. In this mode the envelope and the carrier oscillation of the reference pulse are shifted synchronously, analogous to a mechanical interferometer. Hence this mode yields the interferometric CC. Due to alternating constructive and destructive interference as the reference pulse scans across the sample pulse, the interferometric CC trace oscillates rapidly (cf. Figures 3, 5 and 6). By contrast, in the second mode defined by $\omega_{ref,n}=\omega_n-\omega_0=\delta\omega_n$ $(n=1,2)$ the CC trace exhibits no oscillations at all. In this mode only the envelopes of both colours of the reference pulse are shifted while their carriers remain fixed. Note, that the shape of the reference pulse changes due to the interference of both colours. For $\gamma=0$ the respective carriers of sample and reference pulse are always in phase, so that sample and reference pulse interfere constructively for all delays τ. Therefore, the corresponding CC trace follows the total upper envelope of the interferometric CC (cf. Figures 3 and 6). Analogously, for $\gamma=1$ constant destructive interference of sample and reference pulse yields the total lower envelope of the interferometric CC. This correlation mode is particularly useful for O-LP fields, where both colours are separable by means of their polarization direction. In the other three polarization cases both colours are mixed either due to projection onto the same polarization direction (P-LP case) or due to circular polarization (COR- and CNR-CP case). In these cases another distinct reference frequency for the correlation is given by the centre frequency $\omega_c=(\omega_1+\omega_2)/2$. Hence the third prominent correlation mode is defined by $\omega_{ref,1}=\omega_{ref,2}=\omega_c-\omega_0$. In this mode the CC traces exhibit slow residual oscillations at the frequency $\omega_{beat}=(\omega_2-\omega_1)/2$, indicative of the beating between the two carrier frequencies (cf. Figure 6). Again the choice of γ determines whether the upper $(\gamma=0)$ or lower $(\gamma=1)$ beating envelope is measured.

By adapting the mathematical description of Section 2.1.2, the shaper-based correlation technique can be applied to bichromatic fields of all four polarization states introduced in Section 2.1.1. In the following the technique is discussed specifically for P-LP (case (i)) and O-LP (case (ii)) fields. The remaining cases (iii) and (iv) follow again from additional use of a QWP. Analogous to Equation (3), the target output field for the CC of p-polarized P-LP fields reads

$$\tilde{\boldsymbol{\mathcal{E}}}^{+}_{\text{out,para}}(\omega) = \frac{\mathcal{A}(\omega)}{2}\begin{pmatrix} 0 \\ e^{-i\varphi(\omega)}+e^{-i\varphi_{ref}(\omega)} \end{pmatrix}, \tag{15}$$

with $\varphi(\omega)$ and $\mathcal{A}(\omega)$ as defined in Equation (9). The first term corresponds to the shaped P-LP sample pulse described by Equation (3). The second term describes the P-LP reference pulse, temporally shifted by τ with respect to the sample pulse. The factor 1/2 accounts for the redistribution of the input pulse energy onto two output pulses in this case. The spectral phase modulation functions to generate output fields of the form Equation (15) are given by

$$\varphi_A(\omega) = \frac{1}{2}[\varphi(\omega)+\varphi_{ref}(\omega)] + \operatorname{acos}\left[\frac{\mathcal{A}(\omega)}{\tilde{\mathcal{E}}(\omega)}\cos\left(\frac{\varphi(\omega)-\varphi_{ref}(\omega)}{2}\right)\right] \tag{16}$$

and

$$\varphi_B(\omega) = \frac{1}{2}[\varphi(\omega) + \varphi_{ref}(\omega)] - \operatorname{acos}\left[\frac{\mathcal{A}(\omega)}{\tilde{\mathcal{E}}(\omega)}\cos\left(\frac{\varphi(\omega) - \varphi_{ref}(\omega)}{2}\right)\right]. \tag{17}$$

Similarly, for the CC of O-LP bichromatic fields the target output field reads (cf. Equation (4))

$$\tilde{\boldsymbol{\mathcal{E}}}^{+}_{\mathrm{out,ortho}}(\omega) = \frac{1}{2}\begin{pmatrix}\mathcal{A}_1(\omega)\cdot\left(e^{-i\varphi_1(\omega)} + e^{-i\varphi_{ref}(\omega)}\right)\\ \mathcal{A}_2(\omega)\cdot\left(e^{-i\varphi_2(\omega)} + e^{-i\varphi_{ref}(\omega)}\right)\end{pmatrix}. \tag{18}$$

The spectral phase modulation functions to generate this type of output field are given by

$$\varphi_A(\omega) = \begin{cases}\frac{1}{2}\left[\varphi_1(\omega) + \varphi_{ref}(\omega)\right] - \operatorname{acos}\left[\frac{\mathcal{A}_1(\omega)}{\tilde{\mathcal{E}}(\omega)}\cos\left(\frac{\varphi_1(\omega)-\varphi_{ref}(\omega)}{2}\right)\right], & \omega < 0\\ \frac{1}{2}\left[\varphi_2(\omega) + \varphi_{ref}(\omega)\right] + \operatorname{acos}\left[\frac{\mathcal{A}_2(\omega)}{\tilde{\mathcal{E}}(\omega)}\cos\left(\frac{\varphi_2(\omega)-\varphi_{ref}(\omega)}{2}\right)\right], & \omega \geq 0\end{cases} \tag{19}$$

and

$$\varphi_B(\omega) = \begin{cases}\frac{1}{2}\left[\varphi_1(\omega) + \varphi_{ref}(\omega)\right] - \operatorname{acos}\left[-\frac{\mathcal{A}_1(\omega)}{\tilde{\mathcal{E}}(\omega)}\cos\left(\frac{\varphi_1(\omega)-\varphi_{ref}(\omega)}{2}\right)\right], & \omega < 0\\ \frac{1}{2}\left[\varphi_2(\omega) + \varphi_{ref}(\omega)\right] - \operatorname{acos}\left[\frac{\mathcal{A}_2(\omega)}{\tilde{\mathcal{E}}(\omega)}\cos\left(\frac{\varphi_2(\omega)-\varphi_{ref}(\omega)}{2}\right)\right], & \omega \geq 0\end{cases}. \tag{20}$$

In analogy to interferometer-based CC measurements, application of the spectral phase functions $\varphi_A(\omega)$ and $\varphi_B(\omega)$ in Equations (16), (17), (19) and (20) induce SI fringes, the phase of which is determined by the phase difference between sample and reference pulse.

2.2.2. Angular resolved SI

The complete characterization of the generated polarization-shaped bichromatic fields including the polarization state of both colours requires an additional measurement of the relative (constant) phase between two orthogonal field components. To this end we performed additional Angular Resolved Spectral Interference (ARSI) measurements which reveal the helicity of each colour. Below the concept is discussed on the example of COR-CP and CNR-CP bichromatic fields. The basic idea is to superimpose the sample pulse with a time-delayed replica whose polarization state is inverted. In this case relevant information on the polarization state of the pulse is imprinted in the SI pattern measured under different polar angles α. Experimentally, the ARSI method is realized using a Mach–Zehnder interferometer behind the shaper, equipped with a QWP in each arm (see Figure 7(a)). The QWP in the short arm aligned at $\alpha_1 = \pm 45°$ serves to generate the circularly polarized sample pulse, while the QWP in the long arm aligned at $\alpha_2 = \mp 45°$ prepares the reference pulse with inverted state of polarization. Finally a field component is selected using a rotatable analyzer aligned at α_a and the corresponding spectrum is measured as a function of α_a. We describe this procedure mathematically for the example of a COR-CP bichromatic sample field, i.e. a P-LP field at the shaper output. The Power Spectral Density (PSD) of the pulse sequence measured behind the analyzer is given by

$$\tilde{I}^{+}_{res}(\omega,\alpha_a) \propto \left\| \mathcal{P}_p\, \mathcal{R}(\alpha_a) \times \left[\Lambda_4(\alpha_1) + e^{-i\omega\tau}\Lambda_4(\alpha_2)\right]\tilde{\boldsymbol{\mathcal{E}}}^{+}_{\mathrm{out,para}}(\omega)\right\|^2. \tag{21}$$

For $\alpha_1 = -\alpha_2 = \frac{\pi}{4}$ the sample pulse is left-handed circularly polarized. In this case the measured PSD reads

$$\tilde{I}^{+}_{res}(\omega,\alpha_a) \propto |\tilde{\mathcal{E}}_{\mathrm{out},p}(\omega)|^2 \cdot \left[1 + \cos\left(\omega\tau - 2\alpha_a\right)\right]. \tag{22}$$

This expression describes a two-arm Archimedean spiral which rotates clockwise for increasing values of ω. The rotational sense of the spiral reflects the helicity of the sample pulse, i.e. left-circularly polarized pulses generate clockwise rotating ARSI spirals. In contrast, a right-handed circularly polarized sample pulse generated by $\alpha_1 = -\alpha_2 = -\frac{\pi}{4}$ leads to a anticlockwise rotating spiral described by

$$\tilde{I}^{+}_{res}(\omega,\alpha_a) \propto |\tilde{\mathcal{E}}_{\mathrm{out},p}(\omega)|^2 \cdot \left[1 + \cos\left(\omega\tau + 2\alpha_a\right)\right]. \tag{23}$$

These results hold for any circularly polarized field. In particular, in the cases of COR- and CNR-CP bichromatic fields each colour generates a spectrally separated ARSI spiral, the rotation sense of which directly indicates the helicity of the corresponding colour (cf. Figure 7(c) and (d)). The experimental procedure for the CC and ARSI characterization measurements is described in Section 3.1.

3. Experiment

Here we report on the experimental implementation of the shaper-based scheme for the generation of tailored bichromatic fields. We start in Section 3.1 with a brief description of the experimental setup and procedure. The experimental results are presented in Section 3.2. The generation of P-LP and COR-CP bichromatic fields can be implemented by conventional amplitude and phase shaping (*36*) using standard polarizers. We focus on the shaper-based generation of O-LP and CNR-CP bichromatic fields using a composite polarizer.

3.1. Setup

The unmodulated input pulses required for the shaper-based generation of tailored bichromatic fields were provided by a multipass chirped pulse amplifier (*Femtolasers* Rainbow 500 oscillator with CEP4 module seeding a Femtopower HR 3kHz CEP amplifier) which delivers phase-stabilized laser pulses with a duration of 20 fs and an energy of up to 1.2 mJ. The spectrum is centred around 790 nm with a Full Width at Half Maximum (FWHM) of the intensity of about 80 nm. The temporal characterization of the input pulse was performed by second order autocorrelation measurements using a *Femtolasers* Femtometer and SHG-FROG measurements using a *Swamp Optics* GRENOUILLE (model 8-9 USB). For the generation of bichromatic fields we employed our home-built polarization pulse shaper in 4*f* geometry (*39*) equipped with volume phase holographic transmission gratings (*Wasatch Photonics*, 1500 mm^{-1}) and a dual-layer LC-SLM (*Jenoptik*, SLM-S640d) with 640 pixels per layer. In order to implement bichromatic amplitude modulation we inserted different broadband polarizers (*Codixx*, ColorPol®) behind the LC-SLM and close to the Fourier plane. For the generation of P-LP fields (case (i)) we used a standard polarizer aligned in *p*-direction. O-LP fields (case (ii)) were generated using a composite polarizer with two adjacent active areas with orthogonal transmission directions. The polarizer was adjusted such that the red part of the input spectrum was transmitted in *s*-direction, whereas the blue part was transmitted in *p*-direction (see Figure 1). Conversion to COR-CP (case (iii)) and CNR-CP fields as discussed in Section 3.2.4 was realized by an achromatic QWP (*B. Halle Nachfl.*).

Residual spectral phase compensation was performed prior to the experiments by adaptive optimization of the Second Harmonic Generation (SHG) in a β-barium borate (BBO) crystal (*GWU-Lasertechnik*, $\theta = 29.2°$, 10 µm thickness) (*44*, *45*). In the experiments the detected compensation phases were additionally applied to the LC-SLM to ensure bandwidth-limited output pulses.

In order to characterize the polarization-shaped bichromatic fields we employed a shaper-based spectrally resolved second order CC technique (see also Section 2.2.1). By application of the phase modulation functions in Equations (19) and (20) we generated sequences of a sample pulse and a time-delayed reference pulse with variable delay τ. Both pulses are sent co-linearly into the BBO crystal and the SHG light was detected as a function of τ using a spectrometer (*Avantes*, AVASPEC-ULS3648-RS-USB2, 330–490 nm). Due to the polarization sensitivity of the SHG process the crystal simultaneously acted as analyzer, selecting one polarization component of the generally polarization-shaped sample pulse for characterization. Only in the case of P-LP fields one CC measurement, in our case with the crystal aligned for efficient conversion of *p*-polarized light, is sufficient to characterize the field. For O-LP fields two separate CC measurements with the crystal aligned for efficient *s*- and *p*-conversion, respectively, are required for temporal characterization of the sample pulse. In this case, the characterization is complete except for the relative phase between the *s*- and the *p*-polarization component. This phase however is zero unless altered by polarization-sensitive optical elements, such as dielectric mirrors or birefringent elements. In particular, if a QWP was used to generate circularly polarized bichromatic fields, the CC method was supplemented in order to determine the polarization state of the sample pulse. For this purpose we performed additional ARSI measurements (cf. Section 2.2.2) to fully characterize the COR-CP and CNR-CP fields discussed in Section 3.2.4. The ARSI method was implemented using a Mach–Zehnder interferometer behind the polarization shaper, equipped with a QWP in both the short (sample) and the long (reference) arm (see Figure 7(a)). The QWPs were aligned in orthogonal directions, i.e. at $\alpha_1 = \pm 45°$ and $\alpha_2 \mp 45°$, in order to generate sequences of a circularly polarized bichromatic sample pulse followed by a time-delayed replica with inverted helicity. Behind the interferometer a rotatable analyzer aligned at α_a with respect to the *x*-axis served to select the corresponding field component for detection by a spectrometer (*Avantes*, AVASPEC-ULS3648-USB2, 680–980 nm). By this means we measured the SI of sample and reference pulse for a fixed delay τ as a function of α_a varied between 0° and 180°.

3.2. Results

In order to demonstrate specific advantages of the novel scheme based on a composite polarizer (cf. Section 2.1), we focus on the generation of O-LP and CNR-CP bichromatic fields. We note however, that the basic concept is applicable to P-LP and COR-CP bichromatic fields as

well using conventional polarizers. Figure 2 illustrates prototype bichromatic fields outlining the experimental strategy. We start in Section 3.2.1 with the generation of a bandwidth-limited O-LP bichromatic field as shown schematically in Figure 2(a). For O-LP fields both colours decouple in the laboratory frame representation. Therefore projections of the field in *s*- and *p*-direction reflect the temporal profile of the respective colour. When analyzed in any other basis both colours are mixed, which gives rise to a beating of the two carrier frequencies. Due to this beating – and unlike conventional polarization shaping – the instantaneous polarization of the field undergoes rapid changes seen in the three-dimensional visualization in Figure 2(a). This field serves as a basis from which we explore different degrees of freedom of bichromatic pulse shaping. In Section 3.2.2 we investigate variations of the bichromatic amplitude profile of the O-LP field, including bandwidth, amplitude and central frequency of each colour (cf. Figure 2(b)). Figure 2(c) indicates additional and independent spectral phase modulation of both colours as discussed in Section 3.2.3. Again, since the field is O-LP, the two phase modulations determine the temporal shapes of the *s*- and *p*-component of the resulting temporal field. This greatly facilitates the understanding and rational design of complex polarization-shaped bichromatic fields based on the concepts of conventional spectral phase modulation (*46*, *47*). In Section 3.2.4 we address the generation of CNR-CP bichromatic fields. A bandwidth-limited representative of this class is depicted in Figure 2(d). Due to the circular polarization both colours are no longer separable. In fact any projection of the field exhibits a (phase-shifted) beating pattern in this case. In analogy to the 'single colour' case, the superposition of left- and right-handed circular polarization results in a linear polarization state. In the bichromatic case however the polarization direction rotates constantly about the *z*-axis, lending the field a corkscrew-shaped temporal profile.

3.2.1. Generation of orthogonal linearly polarized bichromatic fields

We start with a proof of principle experiment demonstrating the generation of a bandwidth-limited O-LP bichromatic field (cf. Figure 2(a)). The measured PSD of the field is displayed as solid red line in the top frame of Figure 3. The black dashed line indicates the target spectrum $\mathcal{A}(\omega)$. The input spectrum is shown as grey background. Comparing the spectral shapes of target and measured spectrum reveals the high fidelity of the bichromatic amplitude modulation. For the shape of the target spectrum we chose two Gaussians centred at $\omega_1 = 2.306$ rad/fs and $\omega_2 = 2.450$ rad/fs. Both Gaussians have the same peak amplitudes I_0 (intensity ratio 1:1) and equal FWHM of $\Delta\omega = 0.029$ rad/fs. The composite polarizer was arranged such, that the Gaussian centred around ω_1 (red component) was *s*-polarized while the Gaussian centred at ω_2 (blue component) was *p*-polarized, as indicated by the red and blue circled arrows in Figure 3.

Next we performed a temporal characterization of the generated bichromatic field in a series of spectrally resolved CC measurements based on Equations (19) and (20). The second part of Figure 3 displays a complete data-set acquired during this type of measurements. The results shown in the left column were obtained with the BBO crystal aligned for *s*-conversion. SHG spectra recorded with the BBO crystal aligned for *p*-conversion are shown in the right column. Apparently, the spectra in both columns exhibit only contributions from one of the two Gaussians, i.e. the red component for the *s*-direction and the blue component for the *p*-direction. This confirms the purity of the polarization state of both colours in the O-LP field. In the O-LP case two different CC modes are distinguished (see discussion in Section 2.2.1). By setting $\omega_{ref,1} = \omega_{ref,2} = -\omega_0$ and $\gamma = 0$ in Equation (14) we obtained the interferometric CC shown in the top row of each column in Figure 3. The insets show a magnification of the time window $\Delta\tau = 50$ fs around $\tau = 0$ to resolve the fast oscillations. This time window corresponds to $\Delta\tau \cdot \omega_1/2\pi = 18.4$ oscillation periods for the red and analogously 19.5 periods for the blue component, which is in accordance with the observed number of maxima in the insets. The frames below show the upper and lower envelope of the interferometric CC measured by choosing $\omega_{ref,n} = \delta\omega_n = \omega_n - \omega_0$ $(n = 1, 2)$ and setting $\gamma = 0$ for the upper and $\gamma = 1$ for the lower envelope. In these cases no oscillations are observed. The bottom row displays conventional CC traces obtained by integration along the frequency axis. The temporal durations of $\Delta t \approx 100$ fs extracted from the CC-envelopes are in good agreement with the bandwidth product $\Delta\omega\Delta t \leq 4\ln(2)$ for Gaussian-shaped pulses, indicating the successful compensation of residual spectral phases as described in Section 3.1. The results shown in Figure 3 demonstrate the fidelity of the shaper-based approach to use combined amplitude and phase modulation according to Equations (12) and (13) for the generation and compression of bichromatic fields with specific amplitude profile and well-defined polarization state of each colour.

3.2.2. Amplitude-modulated bichromatic fields

In the next step we investigate the capability of the shaper-based scheme to generate bichromatic amplitude profiles of different shapes. This is of major interest to

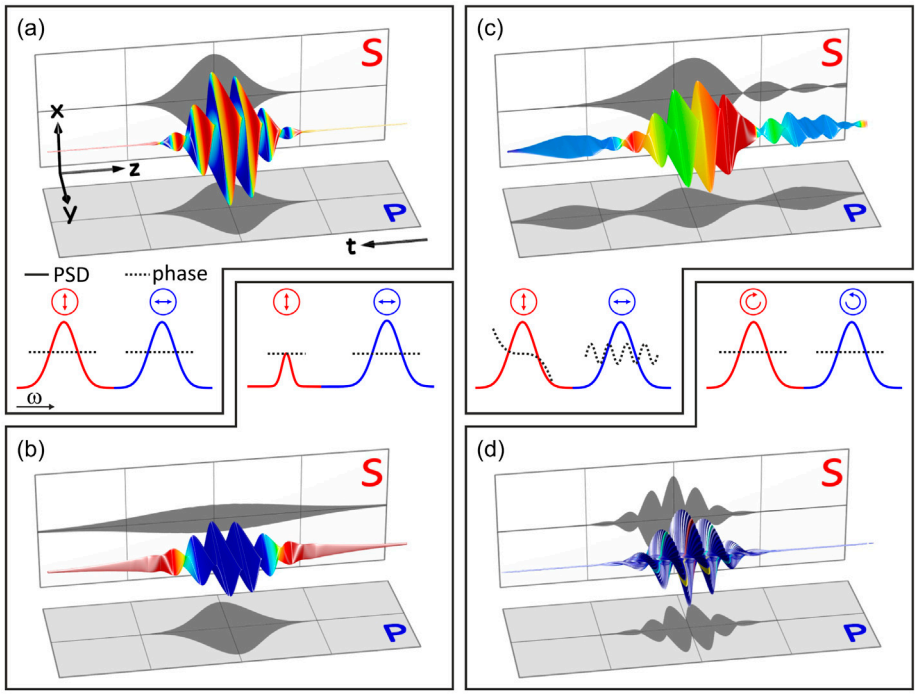

Figure 2. Prototypes of bichromatic fields outlining the experimental strategy. The middle row shows the bichromatic amplitudes (solid lines) and spectral phases (dotted lines) of each colour. The corresponding polarization states are indicated by arrows. The top and bottom row display the resulting temporal fields in terms of the spatio-temporally varying polarization ellipse. Projections along the *x*- and *y*-direction show the temporal profiles of the *p*- and *s*-polarization component, respectively. The colour-coding represents the instantaneous frequency. (a) shows a bandwidth-limited O-LP field based on a symmetric dual-Gaussian spectrum. This field serves as a prototype from which we explore different modes of the shaper-based scheme. (b) shows a variation of the bichromatic amplitude profile realized by decreasing the width and peak amplitude of the red component. This results in a temporal stretching and attenuation of the *s*-polarized field component. (c) displays the result of independent spectral phase modulation of both colours, exemplified on a third order polynomial phase for the red and a sinusoidal phase for the blue component. The effect of each phase function is clearly visible in the corresponding temporal projections. (d) shows a CNR-CP field obtained by sending the field from (a) through a QWP. In this case, the two colours can no longer be disentangled in the temporal projections. Both the *p*- and the *s*-projection of the temporal field display characteristic beating patterns resulting from the mixing of both colours.

applications seeking to control light-matter interactions as it enables precise control of, e.g. the central frequency ratio ($m\omega$ vs. $n\omega$), the intensity ratio ($I_1 : I_2$) and the temporal duration of both colours. Utilizing the amplitude modulation modality of the polarization shaper allows to realize almost any predefined amplitude profile supported by the available bandwidth, which already corresponds to an immense variety of bichromatic waveforms. Specifically, resuming the Gaussian amplitude parameterization introduced in the previous section, the scheme provides full access to all basic parameters, i.e. the spectral position, bandwidth and amplitude, of both Gaussians. Figure 4 shows a collection of Gaussian-shaped bichromatic amplitude profiles with different parameter combinations. The assignment of quantities is the same as in Figure 3. In Figure 4(a) the spectral width of the red component (ω_1) was reduced by a factor of 3 whereas the width of the blue component was increased by the same factor. This results in a bichromatic field with different temporal durations of the two polarization components. The field starts and ends smoothly with the *s*-polarized red component. Only transiently it evolves into a superposition of both colours and, as a consequence, undergoes a rapid change of polarization (cf. Figure 2(b)). This type of fields is particularly useful for applications involving adiabatic state preparation (*48*), adiabatic alignment of molecules (*49*) or materials processing (*50*). In Figure 4(b) the amplitude ratio of the two colours was altered to 1:2 by reducing the amplitude of the red component. By this means the mixing ratio of the two colours can be adjusted in a continuous fashion. Recently, manipulation of the mixing ratio was exploited to control the high harmonic spectrum in attosecond pulse generation using O-LP bichromatic fields (*15*) and to optimize the yield of rescattered electrons in strong-field ionization using CNR-CP bichromatic fields (*51*). Figure 4(c) shows a variation of the central frequency ratio of the bichromatic field. Here the central frequency of the blue component

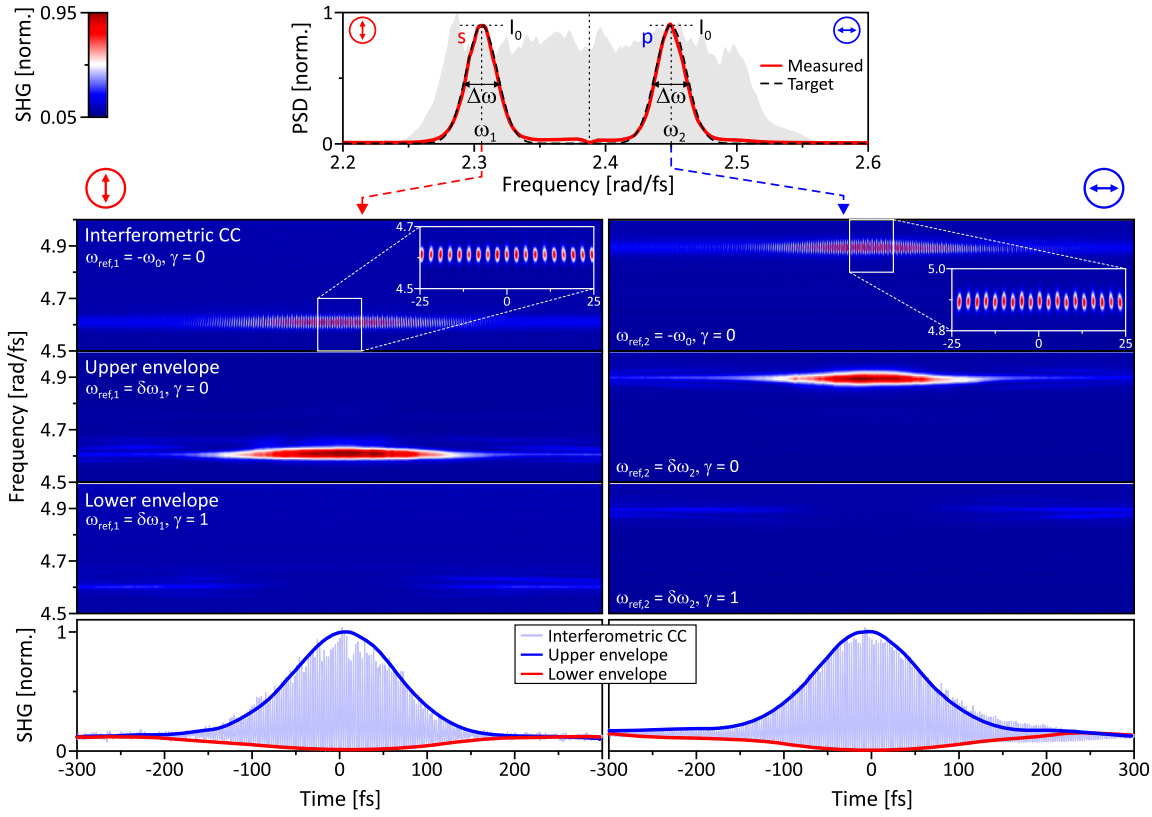

Figure 3. Shaper-based generation of a bandwidth-limited O-LP bichromatic field with symmetric dual-Gaussian amplitude profile (top frame). The two Gaussians are centred around $\omega_1 = 2.306$ rad/fs and $\omega_2 = 2.450$ rad/fs and have the same width $\Delta\omega = 0.029$ rad/fs and peak amplitude I_0. The red component is *s*-, the blue component is *p*-polarized. The fundamental spectrum is depicted as gray background. Middle: Temporal characterization of the bichromatic field via shaper-based spectrally resolved CC measurements of the *s*-component (left column) and the *p*-component (right column). The uppermost row shows interferometric CCs, whereas the two rows below display the corresponding upper and lower envelopes. Integration along the frequency axis yields the conventional CC traces shown in the bottom frame.

was shifted to $\omega_2' = 2.507$ rad/fs. The capability to adjust both central frequencies at will provides spectral tunability. In particular, continuous control of the bichromatic frequency ratio is relevant to applications involving *m*- vs. *n*-photon excitations to study the interference of quantum states with different parity. The results presented in Figure 4 demonstrate the versatility of the shaper-based scheme with respect to the realization of almost any desired bichromatic amplitude profile.

3.2.3. Phase-modulated bichromatic fields

In this section, we demonstrate additional spectral phase modulation of the prototype bichromatic field introduced in Section 3.2.1. Spectral phase modulation provides the option to manipulate the temporal amplitude and phase of the laser pulse without altering its energy content. This is the fundamental basis of coherent control of quantum phenomena, which deals with the manipulation of constructive and destructive interferences of matter waves (*23*, *52*, *53*). The shaper-based scheme provides full control over the spectral phases $\varphi_{1/2}(\omega)$ of the two colours, independent of the choice of the bichromatic amplitude profile $\mathcal{A}_{1/2}(\omega)$ (cf. Figure 2(c)). To demonstrate the independence of those modulations we phase-modulated the *s*-polarized red component by a third-order polynomial $\varphi_1(\omega) = 1.5 \times 10^6\ \mathrm{fs}^3 \cdot (\omega - \delta\omega_1)^3$, while the phase of the *p*-polarized blue component was modulated sinusoidally by $\varphi_2(\omega) = 1.2 \cdot \sin[400\ \mathrm{fs} \cdot (\omega - \delta\omega_2)]$. The spectral detunings are given by $\delta\omega_n = \omega_n - \omega_0$ for $n = 1, 2$. Figure 5 displays the results of the shaper-based CC measurement for the phase-modulated bichromatic field. The blue lines in Figure 5(a) indicate the spectral phase modulation functions (not to scale). Figure 5(b) shows time-resolved CC traces obtained with the BBO crystal aligned for *s*-conversion. The corresponding measured SHG-spectrum shown in the inset exhibits only the red contribution centred around $2\omega_1 = 4.612$ rad/fs. The CC result displays an asymmetric temporal profile which is characteristic for Third Order Dispersion (TOD) (*46*, *47*, *50*). Due to the positive TOD parameter, the field starts with an intense main pulse followed by a series of decaying post-pulses. Quantitatively the envelope of the modulated field is described by an exponentially damped

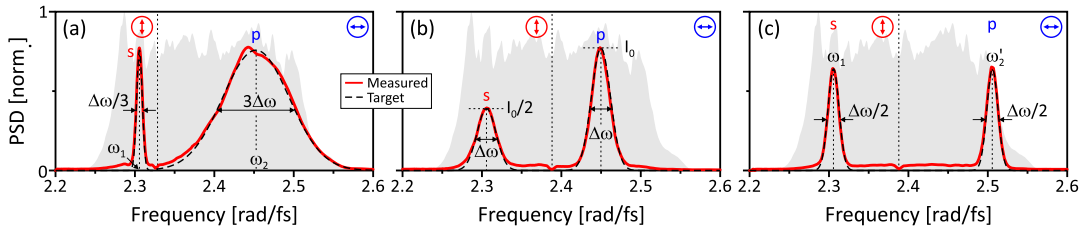

Figure 4. Variation of the bichromatic amplitude profile. The shaper-based approach allows to design any desired amplitude profile supported by the input bandwidth (gray shaded background). In (a) the spectral width of the two Gaussians is varied to generate O-LP fields where with different temporal durations for the *s*- and the *p*-polarization component. (b) shows a variation of the bichromatic amplitude ratio which controls the mixing of the two colours. A variation of the bichromatic frequency ratio is demonstrated in (c). This option provides spectral tunability and, in particular, allows the generation of commensurable bichromatic fields, i.e. so-called $m\omega$-$n\omega$ fields, of adjustable frequency ratio $m:n$.

Airy function. This behaviour is clearly visible in both the upper and the lower envelope of the CC (blue and red line). Characteristic π-jumps in the temporal phase of the modulated field between the sub-pulses due to the zeros of the Airy function are reflected by crossings of the two envelopes. Due to the additional phases of π constructive and destructive interference in the envelope correlation are exchanged leading to an inversion of both envelopes. The CC traces obtained with the BBO crystal aligned for *p*-conversion are shown in Figure 5(c). The SHG spectrum in the inset centred around $2\omega_2 = 4.900$ rad/fs indicates that only the blue component is measured in this case. The CC result displays a typical multi-pulse sequence resulting from sinusoidal phase modulation (*54*, *55*). The sequence consists of a central main pulse preceded and followed by a series of pre- and post-pulses. The amplitude of the *n*th sub-pulse is determined by the Bessel function of first kind and order n, $J_n(A)$, evaluated at the sine-amplitude $A = 1.2$. The temporal separation of the sub-pulses is given by the sine-frequency $T = 400$ fs. Due to the alternating sign $(-1)^n$ of the Bessel functions for $n < 0$ phase-jumps of π occur between adjacent pre-pulses. As a result, the first pre-pulse is in anti-phase with the main pulse as indicated by the inversion of upper and lower envelope for $n = -1$. Note the bandwidth-limited duration of all sub-pulses which indicates that the dispersion management is not affected by the additional spectral phase modulation. Overall the experimental results presented in Figure 5 highlight the capability of the shaper-based scheme to combine bichromatic amplitude modulation and dispersion management with independent spectral phase modulation of both colours. In addition, the scheme provides a powerful means for the accurate temporal characterization of the resulting polarization-shaped bichromatic field. For the detection of the polarization state of both colours the CC technique is supplemented by additional ARSI measurements, which is discussed in the next section on the example of a CNR-CP bichromatic field.

3.2.4. CNR-CP bichromatic fields

So far we discussed the generation of tailored O-LP bichromatic fields. This section is dedicated to the generation and characterization of circularly polarized bichromatic fields. We focus on the example of CNR-CP fields based on the bandwidth-limited prototype discussed in Section 3.2.1. A schematic illustration of the resulting temporal field is shown in Figure 2(d). Experimentally the CNR-CP fields are generated by conversion of the O-LP shaper output field using a QWP aligned at $\alpha = \pm 45°$ behind the shaper output. In the circular case two types of measurements, i.e. a temporal correlation and a SI measurement (see discussion in Section 2.2), are required for a complete characterization. We start with the temporal characterization of the field via shaper-based correlation measurements.

Due to the circular polarization the two colours are mixed in the temporal field. Therefore, unlike the O-LP state (cf. Sections 3.2.1 and 3.2.3) a separate measurement of both colours is not feasible. As discussed in Section 2.2.1, in this case there are three physically meaningful modes for the shaper-based correlation measurement. Figure 6 presents the results from these measurements performed behind the QWP with the BBO crystal aligned for *p*-conversion. The first mode is the interferometric CC obtained by $\omega_{ref,1} = \omega_{ref,2} = -\omega_0$ and $\gamma = 0$. The central frame of Figure 6 shows the spectrally resolved interferometric CC trace. In comparison to the results presented in Figure 3 (right column for the same detection configuration), here contributions from both colours are observed at $2\omega_1$ and $2\omega_2$. In addition, sum frequency generation of the two colours leads to a pronounced mixing term observed at $2\omega_c = \omega_1 + \omega_2 = 4.756$ rad/fs.

The latter displays the temporal beating of the two carrier frequencies at $\omega_{beat} = (\omega_2 - \omega_1)/2 = 0.072$ rad/fs. The corresponding beating period of $T_{beat} = 4\pi/(\omega_2 - \omega_1) = 87$ fs is marked in the spectrally integrated CC traces shown in the bottom frame of Figure 6. Here the results of all three correlation modes are plotted together.

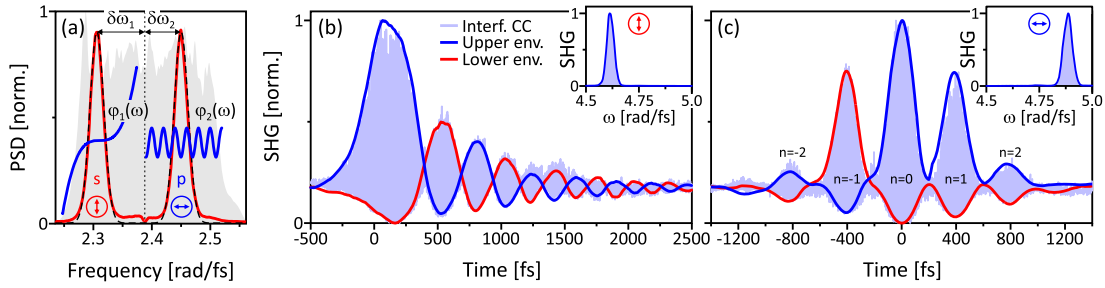

Figure 5. Spectral phase modulation of the O-LP prototype field. (a) qualitatively sketches the phase functions $\varphi_1(\omega) = 1.5 \times 10^6\ \mathrm{fs}^3 \cdot (\omega - \delta\omega_1)^3$ and $\varphi_2(\omega) = 1.2 \cdot \sin[400\ \mathrm{fs} \cdot (\omega - \delta\omega_2)]$ (blue lines) applied to the *s*-polarized red and *p*-polarized blue component, respectively. The result of the phase modulation is seen in the corresponding CC traces shown in (b) and (c). The temporal structure of the *s*-component in (b) displays an Airy-type profile characteristic for third order dispersion. The temporal shape of the *p*-component in (c) describes a multi-pulse sequence typical for periodic phase modulation. The SHG spectra in the insets confirm the polarization contrast of the two colours in the phase-modulated O-LP field.

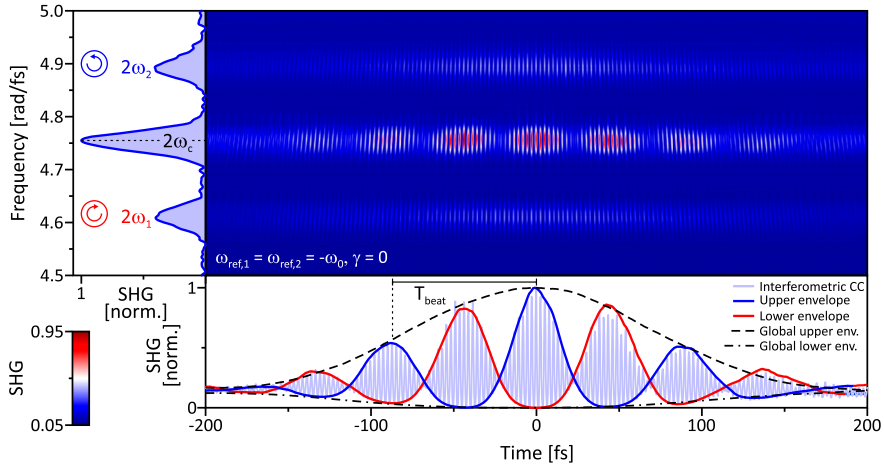

Figure 6. Generation of a bandwidth-limited CNR-CP bichromatic field based on the prototype O-LP field from Figure 3. The spectrally resolved interferometric CC measured in *p*-direction features contributions from both colours centered around $2\omega_1$ and $2\omega_2$, as well as a pronounced mixing term at $2\omega_c = 4.756$ rad/fs. Integration along the time axis yields the SHG spectrum of the sample pulse shown in the left frame. The bottom frame depicts correlation traces from three different modes of the shaper-based CC measurement. The first mode corresponds to the interferometric CC (light-blue solid line) which displays the beating of the two colours with a period of $T_{beat} = 87$ fs. The other two modes correspond to the upper and lower envelope of the beating (red and blue solid lines) and the global upper and lower envelope of the field (black dashed and dash-dotted lines). The respective settings for $\omega_{ref,n}$ and γ are given in the main text.

The second mode corresponds to the upper (blue line) and lower (red line) envelope of the interferometric CC (light-blue line) which are obtained by setting $\omega_{ref,1} = \omega_{ref,2} = \omega_c - \omega_0$ and $\gamma = 0$ and $\gamma = 1$, respectively. The resulting CC traces oscillate slowly at ω_{beat}, providing detailed information on the beating such as the beating period T_{beat} or characteristic π phase jumps which show up as crossings of the two envelopes. In contrast, the third mode obtained by setting $\omega_{ref,n} = \delta\omega_n$ $(n = 1, 2)$ and $\gamma = 0, 1$ (cf. Sections 3.2.1 and 3.2.3) and shown as black dashed and dash-dotted lines in Figure 6 provides information on the global upper and lower envelope of the field which – like in the O-LP case – display no oscillation at all.

Measuring the shaper-based CC for any polarization component of the CNR-CP field yields identical results to those in Figure 6. The technique is therefore not suitable to determine the polarization state of the bichromatic field. Information on the helicity of each colour is imprinted in the ARSI pattern recorded for a fixed delay τ between sample and reference pulse (cf. Section 2.2.2). The optical setup used for the ARSI measurements is shown in Figure 7(a). In a first step we calibrated the method by means of a well-characterized sequence of unmodulated laser pulses. The sequence was generated by removing the polarizer in the Fourier plane (no amplitude modulation) and using the LC-SLM to apply linear phases $\varphi_{A/B}(\omega) = \mp\frac{\tau}{2} \cdot \omega$ to the shaper frame

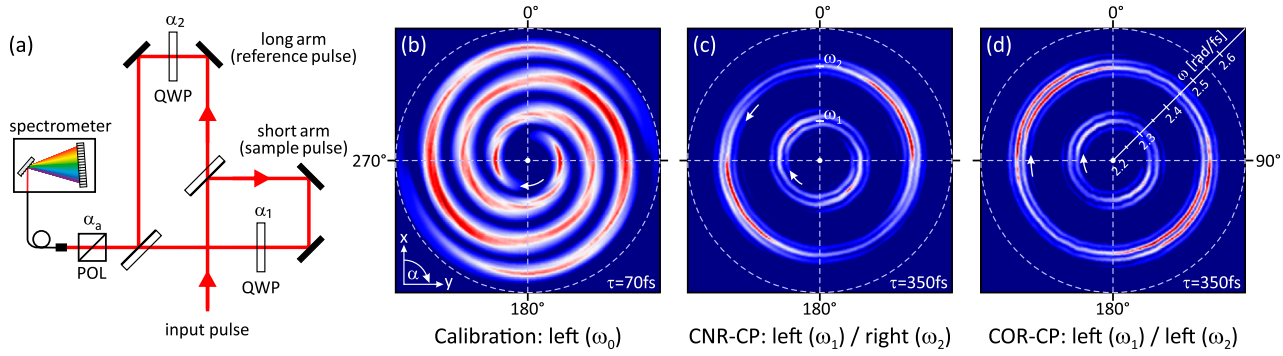

Figure 7. Polarization state characterization using the ARSI technique. (a) diagnostic setup consisting of a Mach–Zehnder interferometer equipped with QWPs in each arm, aligned at angle α_1 (sample pulse) and α_2 (reference pulse). The ARSI traces are recorded by measuring the spectrum of the pulse sequence as function of the angle α_a of the rotatable analyzer POL. (b) Calibration of the method by means of an unmodulated left-handed circularly polarized sample pulse. The measured interference pattern describes a clockwise rotating Archimedian spiral. (c) ARSI measurement of the bandwidth-limited CNR-CP prototype field. In this case two interleaved spirals are observed corresponding to the two colours of the bichromatic field. The inner spiral with radius ω_1 rotates clockwise, whereas the outer spiral with radius ω_2 rotates counter-clockwise. Thus the sample pulse is a left–right CNR-CP bichromatic field. (d) ARSI measurement of bandwidth-limited COR-CP bichromatic field. Here both spirals rotate clockwise indicating a left-left COR-CP sample pulse.

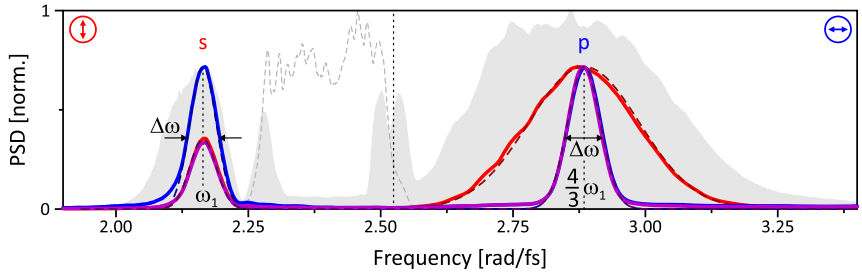

Figure 8. Initial results on the shaper-based generation of commensurable bichromatic fields extracted from a WLS (gray-shaded background) by amplitude modulation. The WLS was generated using an Argon-filled hollow core fibre compressor (gas pressure $p \approx 1$bar) seeded by the amplifier pulse (pulse energy $E \approx 100\,\mu$J; gray dashed line). The polarization shaper was adapted to the ultrabroad WLS by using suitable transmission gratings (*Wasatch Photonics*, 650mm^{-1}). The figure shows three dual-Gaussian spectra centered around $\omega_1 = 2.17$ rad/fs and $\omega_2 = 4\omega_1/3 = 2.89$ rad/fs. For the blue spectrum the amplitudes and widths of the two Gaussians were chosen to be equal, with $\Delta\omega = 0.06$ rad/fs. In case of the magenta spectrum the amplitude of the low-frequency component was reduced by a factor of 2. For the red spectrum the width of the high-frequency Gaussian was additionally increased by a factor of 3.4. These results demonstrate high-fidelity generation of bichromatic amplitude profiles with commensurable frequencies (here 3ω vs. 4ω) via the shaper-based approach.

components of the input pulse. For $\tau > 0$ this results in a pulse pair consisting of a first pulse polarized under 45° (LCD A) and the second, time-delayed pulse polarized under 135° (LCD B) with respect to the x-axis. Using a QWP aligned at $\alpha = 0°$ (cf. Equation (10)) delivers sequences of a left-handed circularly polarized sample pulse followed by a right-handed circularly polarized reference pulse, according to the handedness conventions used in (*56*). The time delay was set to $\tau = 70$ fs which results in about $\tau/\Delta t \approx 3$ visible interference fringes over the full range of the input spectrum. As shown in Figure 7(b) this calibration pulse sequence generated an ARSI spiral with clockwise sense of rotation. Thus, in accordance with Equations (22) and (23) clockwise rotating ARSI spirals are associated with left-handed circularly polarized sample pulses, whereas right-handed circularly polarized sample pulses create counter-clockwise ARSI spirals. Next we applied the technique to the CNR-CP field discussed in Figure 6. Taking into account the reduced spectral bandwidth of both colours the delay was increased to $\tau = 350$ fs in order to roughly maintain the number of visible fringes over the corresponding spectral ranges. Figure 7(c) shows the experimental results obtained with the QWPs in the short and long arm of the interferometer aligned at $\alpha_1 = -45°$ and $\alpha_2 = 45°$, respectively. The recorded ARSI pattern shows two separate spirals corresponding to the two colours of the bichromatic field. The inner spiral with radius ω_1 rotates clockwise indicating that the red component is left-handed circularly polarized. In contrast, the blue

component is right-handed circularly polarized as indicated by the anticlockwise rotation of the outer spiral with radius ω_2. Figure 7(d) displays the ARSI pattern of a COR-CP bichromatic field generated using a standard polarizer with transmission axis in p-direction behind the LC-SLM. In this case the QWPs were aligned at $\alpha_1 = 45°$ and $\alpha_2 = -45°$, respectively. According to the clockwise rotation sense of both ARSI spirals, this configuration leads to a COR-CP bichromatic field where both colours are left-handed circularly polarized.

4. Summary and outlook

In this contribution we have introduced an effective route to the generation of ultrashort bichromatic laser fields with tailored amplitude, phase and polarization profile. Our scheme utilizes a polarization pulse shaper in amplitude and phase modulation mode to sculpture the desired bichromatic amplitude profile from a given input spectrum. The use of different types of polarizers allows generation of either P-LP (conventional polarizer) or O-LP (composite polarizer) bichromatic fields. Conversion to COR-CP and CNR-CP fields is achieved by application of a QWP at the shaper output. We demonstrated the shaper-based approach experimentally on the example of O-LP and CNR-CP bichromatic fields. In a series of four experiments we first verified the working principle of the scheme by generation of a prototype O-LP bichromatic field. The field was characterized employing a shaper-based spectrally resolved CC technique. Next we highlighted the versatility of the scheme in terms of (1) bichromatic amplitude shaping and (2) independent spectral phase modulation of both colours. The results emphasize the high fidelity achieved in the shaper-based generation of tailored bichromatic fields. Finally, control of the polarization state was demonstrated by generation of COR-CP and CNR-CP bichromatic fields using an additional QWP. For the determination of the field's polarization state we employed an ARSI method which revealed the helicity of both colours. The experimental results show that the shaper-based approach provides full control over all bichromatic parameters, such as the central frequency ratio, the mixing ratio, the bandwidth and the polarization state of each colour, and especially allows to tailor both colours individually in terms of spectral amplitude and phase. In addition, the scheme features built-in dispersion management and the capability for temporal characterization of the generated fields by means of shaper-based CC and SI measurements.

The power of polarization-shaped bichromatic fields is based on the ability to adjust selected spectral bands with sufficient bandwidth for pulse shaping and a specific state of polarization to atomic or molecular transitions. Ultrafast polarization-shaped bichromatic fields provide a route to multi-colour coherent control schemes for the choice and the discrimination of specific quantum pathways via selection rules and resonances. Currently, we study the generation of ultrashort tailored few-cycle bichromatic fields with (low order) commensurable frequencies, so-called $m\omega$ vs. $n\omega$ fields. To this end we apply the shaper-based scheme to a WLS from a noble-gas-filled hollow core fibre compressor. This type of fields has recently emerged as a new twist to control the time-evolution of free electron wave packets from strong-field ionization of atoms (*9*, *10*, *13*, *17*). Initial results on bichromatic amplitude modulation of a WLS from an Argon-filled hollow fibre compressor are shown in Figure 8 (see figure caption for details). The WLS ideally supports the generation of 3ω vs. 4ω fields. Other frequency ratios are possible for different parameter combinations of the WLS generation. Preliminary investigations on the Carrier Envelope Phase (CEP) stability of the generated bichromatic fields indicate that the shaper setup introduces less than 100 mrad (root mean square) of additional CEP noise measured over a period of 200 ms. The availability of CEP-stable few-cycle bichromatic fields with adjustable amplitude, phase and polarization profiles will open up new perspectives for the coherent control of ultrafast electron dynamics. In particular, we will study the control of photoelectron angular distributions via interference of quantum states with different parity induced by n- vs. m-photon ionization.

Disclosure statement

No potential conflict of interest was reported by the authors.

Funding

Financial support by the Deutsche Forschungsgemeinschaft (DFG) via the priority programme [SPP1840-QUTIF] is gratefully acknowledged. Furthermore we thank Jens Köhler from the group of Prof. Thomas Baumert (University of Kassel) for stimulating discussions in the early stage of the project.

References

(1) Kling, M.F.; Vrakking, M.J.J. Attosecond Electron Dynamics. *Ann. Rev. Phys. Chem.* **2008,** *59,* 463–499.
(2) Krausz, F.; Ivanov, M. Attosecond Physics. *Rev. Mod. Phys.* **2009,** *81,* 163–234.
(3) Wirth, A.; Hassan, M.T.; Grguras, I.; Gagnon, J.; Moulet, A.; Luu, T.T.; Pabst, S.; Santra, R.; Alahmed, Z.A.; Azzeer, A.M.; Yakovlev, V.S.; Pervak, V.; Krausz, F.; Goulielmakis, E. Synthesized Light Transients. *Science* **2011,** *334,* 195–200.
(4) Abel, M.; Neumark, D.M. Leone S. R., and T. Pfeifer. Classical and Quantum Control of Electrons Using the

Carrier-envelope Phase of Strong Laser Fields. *Laser Photonics Rev.* **2011,** *5,* 352–367.
(5) Bayer, T.; Braun, H.; Sarpe, C.; Siemering, R.; von den Hoff, P.; de Vivie-Riedle, R.; Baumert, T.; Wollenhaupt, M. Charge Oscillation Controlled Molecular Excitation. *Phys. Rev. Lett.* **2013,** *110,* 123003.
(6) Shafir, D.; Mairesse, Y.; Villeneuve, D.M.; Corkum, P.B.; Dudovich, N. Atomic Wavefunctions Probed Through Strong-field Light-matter Interaction. *Nat. Phys.* **2009,** *1251,* 412–416.
(7) Xie, X.H.; Roither, S.; Grafe, S.; Kartashov, D.; Persson, E.; Lemell, C.; Zhang, L.; Schoffler, M.S.; Baltuska, A.; Burgdorfer, J.; Kitzler, M. Probing the Influence of the Coulomb Field on Atomic Ionization by Sculpted Two-color Laser Fields. *New J. Phys.* **2013,** *15.*
(8) Zhang, L.; Xie, X.H.; Roither, S.; Zhou, Y.M.; Lu, P.X.; Kartashov, D.; Schoffler, M.; Shafir, D.; Corkum, P.B.; Baltuska, A.; Staudte, A.; Kitzler, M. Subcycle Control of Electron-electron Correlation in Double Ionization. *Phys. Rev. Lett.* **2014,** *112,* 193002.
(9) Richter, M.; Kunitski, M.; Schoffler, M.; Jahnke, T.; Schmidt, L.P.H.; Li, M.; Liu, Y.Q.; Dorner, R. Streaking Temporal Double-slit Interference by an Orthogonal Two-color Laser Field. *Phys. Rev. Lett.* **2015,** *114,* 143001.
(10) Mancuso, C.A.; Hickstein, D.D.; Grychtol, P.; Knut, R.; Kfir, O.; Tong, X.M.; Dollar, F.; Zusin, D.; Gopalakrishnan, M.; Gentry, C.; Turgut, E.; Ellis, J.L.; Chen, M.C.; Fleischer, A.; Cohen, O.; Kapteyn, H.C.; Murnane, M.M. Strong-field ionization with two-color circularly polarized laser fields. *Phys. Rev. A* **2015,** *91,* 031402R.
(11) Corkum, P.B.; Burnett, N.H.; Yu Ivanov, M. Subfemtosecond Pulses. *Opt. Lett.* **1994,** *19,* 1870–1872.
(12) Eichmann, H.; Egbert, A.; Nolte, S.; Momma, C.; Wellegehausen, B.; Becker, W.; Long, S.; McIver, K. Polarization-dependent High-order Two-color Mixing. *Phys. Rev. A* **1995,** *51* (5), R3414–R3417.
(13) Milosevic, D.B.; Becker, W.; Kopold, R. Generation of Circularly Polarized High-order Harmonics by Two-color Coplanar Field Mixing. *Phys. Rev. A* **2000,** *61* (6), 063403.
(14) Kitzler, M.; Lezius, M. Spatial Control of Recollision Wave Packets with Attosecond Precision. *Phys. Rev. Lett.* **2005,** *95,* 253001.
(15) Dudovich, N.; Smirnova, O.; Levesque, J.; Mairesse, Y.; Ivanov, M.Y.; Villeneuve, D.M.; Corkum, P.B. Measuring and Controlling the Birth of Attosecond XUV pulses. *Nature Phys.* **2006,** *2,* 781–786.
(16) Pisanty, E.; Sukiasyan, S.; Ivanov, M. Spin Conservation in High-order-harmonic Generation Using Bicircular Fields. *Phys. Rev. A* **2014,** *90,* 043829.
(17) Kfir, O.; Grychtol, P.; Turgut, E.; Knut, R.; Zusin, D.; Popmintchev, D.; Popmintchev, T.; Nembach, H.; Shaw, J.M.; Fleischer, A.; Kapteyn, H.; Murnane, M.; Cohen, O. Generation of Bright Phase-matched Circularly-polarized Extreme Ultraviolet High Harmonics. *Nat. Phot.* **2015,** *9,* 99–105.
(18) Thompson, M.; Thomas, M. Taday P., T. Posthumus, A. Langley, L. Frasinski, and K. Codling. One and Two-colour Studies of the Dissociative Ionization and Coulomb Explosion of h_2 with Intense ti:sapphire Laser Pulses. *J. Phys. B* **1997,** *30,* 5755–5772.
(19) Ray, D.; He, F.; De, S.; Cao, W.; Mashiko, H.; Ranitovic, P.; Singh, K.P.; Znakovskaya, I.; Thumm, U.; Paulus, G.G.; Kling, M.F.; Litvinyuk, I.V.; Cocke, C.L. Ion-energy Dependence of Asymmetric Dissociation of d-2 by a Two-color Laser Field. *Phys. Rev. Lett.* **2009,** *103.*
(20) Dupont, E.; Corkum, P.B.; Liu, H.C.; Buchanan, M.; Wasilewski, Z.R. Phase-controlled Currents in Semiconductors. *Phys. Rev. Lett.* **1995,** *74,* 3596–3599.
(21) Costa, L.; Betz, M.; Spasenovic, M.; Bristow, A.D.; Van Driel, H.M. All-optical Injection of Ballistic Electrical Currents in Unbiased Silicon. *Nat. Phys.* **2007,** *3* (9), 632–635.
(22) Güdde, J.; Rohleder, M.; Meier, T.; Koch, S.W.; Höfer, U. Controlled Electric Currents at a Metal Surface Time-resolved Investigation of Coherently. *Science* **2007,** *318,* 1287–1291.
(23) Shapiro, M.; Brumer, P. *Quantum Control of Molecular Processes*, Vol. 2, Wiley-VCH: Berlin, 2011. pp. 1–544.
(24) Lozovoy, V.V.; Pastirk, I.; Dantus, M. Multiphoton Intrapulse Interference. iv. Ultrashort Laser Pulse Spectral Phase Characterization and Compensation. *Opt. Lett.* **2004,** *29,* 1–3.
(25) von Vacano, B.; Buckup, T.; Motzkus, M. In Situ Broadband Pulse Compression for Multiphoton Microscopy Using a Shaper-assisted Collinear Spider. *Opt. Lett.* **2006,** *31,* 1154–1156.
(26) Plewicki, M.; Weise, F.; Weber, S.M.; Lindinger, A. Phase, Amplitude, and Polarization Shaping with a Pulse Shaper in a Mach-zehnder Interferometer. *Appl. Opt.* **2006,** *45,* 8354–8359.
(27) Ninck, M.; Galler, A.; Feurer, T.; Brixner, T. Programmable Common-path Vector Field Synthesizer for Femtosecond Pulses. *Opt. Lett.* **2007,** *32,* 3379–3381.
(28) Galler, A.; Feurer, T. Pulse Shaper Assisted Short Laser Pulse Characterization. *Appl. Phys. B* **2008,** *90,* 427–430.
(29) Brixner, T.; Gerber, G. Femtosecond polarization pulse shaping. *Opt. Lett.* **2001,** *26,* 557–559.
(30) Wefers, M.M.; Nelson, K.A. Generation of High-fidelity Programmable Ultrafast Optical Waveforms. *Optt. Lett.* **1995,** *20,* 1047–1049.
(31) Weiner, A.M. Femtosecond Pulse Shaping Using Spatial Light Modulators. *Rev. Sci. Instr.* **2000,** *71,* 1929–1960.
(32) Polachek, L.; Oron, D.; Silberberg, Y. Full Control of the Spectral Polarization of Ultrashort Pulses. *Opt. Lett.* **2006,** *31,* 631–633.
(33) Weise, F.; Lindinger, A. Full Control Over the Electric Field Using Four Liquid Crystal Arrays. *Opt. Lett.* **2009,** *34,* 1258–12560.
(34) Kupka, D.; Schlup, P.; Bartels, R.A. Simplified Ultrafast Pulse Shaper for Tailored Polarization States Using a Birefringent Prism. *Rev. Sci. Instr.* **2009,** *80,* 053110.
(35) Schwarz, C.; Huter, O.; Brixner, T. Full Vector-field Control of Ultrashort Laser Pulses Utilizing a Single Dual-layer Spatial Light Modulator in a Common-path Setup. *JOSA B* **2015,** *32,* 933–945.
(36) Weiner, A.M. Ultrafast Optical Pulse Shaping: A Tutorial Review. *Opt. Commun.* **2011,** *284,* 3669–3692.
(37) Oron, D.; Dudovich, N.; Silberberg, Y. In Femtosecond Phase-and-polarization Control for Background-free Coherent Anti-stokes Raman Spectroscopy. *Phys. Rev. Lett.*, **2003**. *90,* pp. 213902-1–213902-4.

(38) Brixner, T.; Krampert, G.; Pfeifer, T.; Selle, R.; Gerber, G.; Wollenhaupt, M.; Graefe, O.; Horn, C.; Liese, D.; Baumert, T. Quantum Control by Ultrafast Polarization Shaping. *Phys. Rev. Lett.* **2004,** *92,* 208301.
(39) Wollenhaupt, M.; Krug, M.; Köhler, J.; Bayer, T.; Sarpe-Tudoran, C.; Baumert, T. Photoelectron Angular Distributions from Strong-field Coherent Electronic Excitation. *Appl. Phys. B* **2009,** *95,* 245–259.
(40) Monmayrant, A.; Chatel, B. New Phase and Amplitude High Resolution Pulse Shaper. *Rev. Sci. Instr.* **2004,** *75,* 2668–2671.
(41) Dudovich, N.; Oron, D.; Silberberg, Y. Quantum Control of the Angular Momentum Distribution in Multiphoton Absorption Processes. *Phys. Rev. Lett.* **2004,** *92,* 103003.
(42) Köhler, J.; Wollenhaupt, M.; Bayer, T.; Sarpe, C.; Baumert, T. Zeptosecond Precision Pulse Shaping. *Opt. Express* **2011,** *19,* 11638–11653.
(43) Keusters, D.; Tan, H.S.; O'Shea, P.; Zeek, E.; Trebino, R.; Warren, W.S. Relative-phase Ambiguities in Measurements of Ultrashort Pulses with Well-separated Multiple Frequency Components. *JOSA B* **2003,** *20,* 2226–2237.
(44) Baumert, T.; Brixner, T.; Seyfried, V.; Strehle, M.; Gerber, G. Femtosecond Pulse Shaping by an Evolutionary Algorithm with Feedback. *Appl. Phys. B* **1997,** *65,* 779–782.
(45) Meshulach, D.; Yelin, D.; Silberberg, Y. Adaptive Ultrashort Pulse Compression and Shaping. *Opt. Comm.* **1997,** *138,* 345–348.
(46) Wollenhaupt, M.; Assion, A.; Baumert, T. In Short and Ultrashort Laser Pulses. *Handbook of Lasers and Optics*, Springer; 2012. pp. 1047–1094.
(47) Wollenhaupt, M.; Bayer, T.; Baumert, T. In Control of Ultrafast Electron Dynamics with Shaped Femtosecond Laser Pulses: From Atoms to Solids. *Book Section 4*, Springer: 2015. pp. 63–122.
(48) Bayer, T.; Wollenhaupt, M.; Sarpe-Tudoran, C.; Baumert, T. Robust Photon Locking. *Phys. Rev. Lett.* **2009,** *102,* 023004.
(49) Guérin, S.; Rouzée, A.; Hertz, E. Ultimate Field-free Molecular Alignment by Combined Adiabatic-impulsive Field Design. *Phys. Rev. A* **2008,** *77,* 041404(R)-1–041404(R)-4.
(50) Englert, L.; Rethfeld, B.; Haag, L.; Wollenhaupt, M.; Sarpe-Tudoran, C.; Baumert, T. Control of Ionization Processes in High Band Gap Materials via Tailored Femtosecond Pulses. *Opt. Express* **2007,** *15,* 17855–17862.
(51) Mancuso, C.A.; Hickstein, D.D.; Dorney, K.M.; Ellis, J.L.; Hasovic, E.; Knut, R.; Grychtol, P.; Gentry, C.; Gopalakrishnan, M.; Zusin, D.; Dollar, F.J.; Tong, X.M.; Milosevic, D.B.; Becker, W.; Kapteyn, H.C.; Murnane, M.M. Controlling Electron-ion Rescattering in Two-color Circularly Polarized Femtosecond Laser Fields. *Phys. Rev. A* **2016,** *93,* 053406.
(52) Rice, S.A.; Zhao, M. *Optical Control of Molecular Dynamics*; Wiley, New York, 2000.
(53) Tannor, D. *Introduction to Quantum Mechanics: A Time-Dependent Perspective*, Palgrave Macmillan Publishers Limited; 2007. p. 600.
(54) Wollenhaupt, M.; Präkelt, A.; Sarpe-Tudoran, C.; Liese, D.; Bayer, T.; Baumert, T. Femtosecond Strong-field Quantum Control with Sinusoidally Phase-modulated Pulses. *Phys. Rev. A* **2006,** *73,* 063409.
(55) Bayer, T.; Wollenhaupt, M.; Baumert, T. Strong-field Control Landscapes of Coherent Electronic Excitation. *J. Phys. B* **2008,** *41,* 074007-1–074007-13.
(56) Born, M.; Wolf, E. *Principles of Optics*, University Press: Cambridge, 1999. pp. 1–952.